Electron Dynamics in the Core-Excited CS 2 Molecule Revealed through Resonant Inelastic X-Ray Scattering Spectroscopy

T Marchenko, S Carniato, L Journel, R Guillemin, E Kawerk, M Žitnik, M Kavčič, K Bučar, R Bohinc, M Petric, et al.

Electron Dynamics in the Core-Excited CS₂ Molecule Revealed through Resonant Inelastic X-Ray Scattering Spectroscopy

T. Marchenko,[1,2,*] S. Carniato,[1,2] L. Journel,[1,2] R. Guillemin,[1,2] E. Kawerk,[1,2,3] M. Žitnik,[4] M. Kavčič,[4] K. Bučar,[4] R. Bohinc,[4] M. Petric,[4] V. Vaz da Cruz,[5] F. Gel'mukhanov,[5,6] and M. Simon[1,2]

[1]*CNRS, UMR7614, Laboratoire de Chimie Physique-Matière et Rayonnement, F-75005 Paris, France*
[2]*Sorbonne Universités, UPMC Univ Paris 6, UMR7614,*
Laboratoire de Chimie Physique-Matière et Rayonnement, F-75005 Paris, France
[3]*Université Libanaise, Faculté des Sciences II Fanar, Laboratoire de Physique Appliquée,*
90656 Jdeidet el Metn, Lebanon
[4]*Jožef Stefan Institute, SI-1001 Ljubljana, Slovenia*
[5]*Theoretical Chemistry & Biology, School of Biotechnology,*
Royal Institute of Technology, SE-106 91 Stockholm, Sweden
[6]*Synchrotron SOLEIL, l'Orme des Merisiers, Saint-Aubin, BP 48, 91192 Gif-sur-Yvette Cedex, France*

We present an experimental and theoretical study of resonant inelastic x-ray scattering (RIXS) in the carbon disulphide CS₂ molecule near the sulfur K-absorption edge. We observe a strong evolution of the RIXS spectral profile with the excitation energy tuned below the lowest unoccupied molecular orbital (LUMO) absorption resonance. The reason for this is twofold. Reducing the photon energy in the vicinity of the LUMO absorption resonance leads to a relative suppression of the LUMO contribution with respect to the emission signal from the higher unoccupied molecular orbitals, which results in the modulation of the total RIXS profile. At even larger negative photon-energy detuning from the resonance, the excitation-energy dependence of the RIXS profile is dominated by the onset of electron dynamics triggered by a coherent excitation of multiple electronic states. Furthermore, our study demonstrates that in the hard x-ray regime, localization of the S 1s core hole occurs in CS₂ during the RIXS process because of the orientational dephasing of interference between the waves scattering on the two sulfur atoms. Core-hole localization leads to violation of the symmetry selection rules for the electron transitions observed in the spectra.

Subject Areas: Atomic and Molecular Physics,
                                                                                             Chemical Physics

I. INTRODUCTION

Excitation of a molecule with a high-energy photon leads to an ultrafast dynamic response involving nuclear and electronic degrees of freedom. A translational, vibrational, and rotational nuclear motion occurs on the femtosecond scale (1 fs = 10^{-15} s), whereas the time scale of electron dynamics is on the order of attoseconds (1 as = 10^{-18} s). Alternatively to the time-resolved measurements using ultrafast laser sources, the nuclear and electron dynamics can be successfully studied in the x-ray energy domain using a technique known as "core-hole clock" spectroscopy based on core-level excitation and decay. This method uses the lifetime of the intermediate core-hole state as an internal reference clock for the temporal evolution of different processes like ultrafast dissociation of core-excited

*[*]tatiana.marchenko@upmc.fr

molecules [1] and electron transfer at the interface between the substrate and the adsorbed gas-phase molecules [2]. The short lifetime of deep core-hole states, accessible with hard x-ray radiation, prevents molecules from changing their orientation during x-ray scattering, which allows one to obtain detailed information on the anisotropy of molecular orbitals using polarized x-ray fluorescence [3].

With respect to nonresonant methods of x-ray spectroscopy [4], the resonant core-hole clock technique brings an additional control knob—photon-energy detuning Ω from the absorption resonance [5–7]. It has been established that inverse detuning characterizes the so-called "scattering duration time" [8,9], which appeared to be a powerful tool in studies of bound [8] and dissociative states [10,11]. Therefore, the dependence of the spectral profile on the excitation-energy detuning allows one to map the temporal evolution of the electron and/or nuclear wave packets, controlled by the scattering duration time. The natural lifetime of the core hole gives the upper limit of the detuning-dependent scattering duration time under the resonant conditions, when Ω = 0.

The decay of an excited molecule occurs through emission of an Auger electron or an x-ray photon. The

corresponding core-hole clock techniques are referred to as resonant Auger electron spectroscopy and resonant inelastic x-ray scattering (RIXS). Both techniques have shown their strong potential for probing nuclear and electronic degrees of freedom in molecules, liquids, and solids [12–14].

Observation of electron dynamics using resonant Auger electron spectroscopy was reported in solid-state studies. Electron transfer from the adsorbed atoms and molecules to the substrate [15,16] and electron delocalization in DNA pressed to a solid substrate [17] were shown to occur on the attosecond time scale.

Our previous studies in gas-phase molecules excited at the iodine L shell [18] and the chlorine K shell [19–24] show that spectral features of RIXS and resonant Auger electron emission carry information on subfemtosecond nuclear dynamics in a molecule upon core-hole excitation. Nonlinear dispersion and a significant narrowing of the spectral lines around the resonant excitation were shown to reflect molecular bond elongation. To our knowledge, so far there have been no attempts to reveal the electron dynamics in isolated molecules using core-hole clock spectroscopy.

In this paper, we report on the strong evolution of the RIXS profile with detuning below the first absorption resonance in the carbon disulphide CS_2 molecule excited at the sulfur K shell. The experimental results are presented in Sec. II. First, we interpret the presence of a symmetry-forbidden transition dominating the RIXS spectrum as due to localization of the S 1s core hole. The mechanism of the core-hole localization, and hence, of symmetry breaking, is specific to the hard x-ray regime and is related to the orientational dephasing of interference in randomly oriented CS_2 molecules (Sec. III). This interpretation is corroborated by the agreement of the experimental data with our *ab initio* calculations considering core-excited states with a localized core hole (Sec. IV). Second, the *ab initio* calculations allow one to reveal the origin of the observed unexpected evolution of the RIXS profile with the excitation photon energy. The mechanism discussed in Sec. V relates the experimentally observed dependence of the RIXS spectra on the photon-energy detuning to the varying partial contributions of the intermediate core-excited states. Finally, our calculations demonstrate that the evolution of the RIXS profile at large detuning of the excitation energy below the absorption resonance reflects the temporal evolution of the multielectron wave packet in the presence of a deep S 1s core hole (Sec. VI). This electron dynamics originates from interference of coherently excited multielectron core-hole states and is interpreted through the interplay between the effective scattering duration and the characteristic time of the core-excited electronic wave-packet evolution. Our main findings are summarized in Sec. VII.

II. EXPERIMENTAL RESULTS

The core-valence configuration of the singlet ground state of carbon disulphide CS_2 [25] is $(1\sigma_g)^2(1\sigma_u)^2\dots$

$(5\sigma_g)^2(4\sigma_u)^2(6\sigma_g)^2(5\sigma_u)^2(2\pi_u)^4(2\pi_g)^4$. The measured S K_β RIXS spectra result from the excitation of the S 1s electrons to the unoccupied molecular orbitals (MO) accompanied by the decay of the valence-shell electrons to the S 1s core hole and the emission of an x-ray photon.

The measurements were performed at the ID26 beam line at the European Synchrotron Radiation Facility (ESRF). The experimental setup is described in detail in Ref. [26]. Essentially, a linearly polarized focused beam with a $250 \times 50 \ \mu m^2$ cross section passes through a stainless-steel gas cell separated from vacuum by 12.5-μm-thick kapton windows and filled with CS_2 vapor at a pressure of 10 mbar. Scattered photons were collected by employing a crystal spectrometer in Johansson geometry with a 500-mm Rowland circle radius using the first-order reflection of a Si(111) crystal. The polarization vectors and the momenta of incident and scattered photons are mutually orthogonal. The diffracted photons were detected with a thermoelectrically cooled (−40 °C) CCD camera with $22.5 \times 22.5 \ \mu m^2$ pixel size. The incident radiation with a bandwidth of around 0.2 eV half width at half maximum (HWHM) was tuned with a 0.2-eV step in the 2468–2480-eV energy range. Figure 1 shows the measured partial x-ray fluorescence yield of the sulfur K hole in CS_2 with the assignment of the lowest absorption bands, which correspond to the excitation from the S 1s shell to the lowest unoccupied molecular orbital (LUMO) $(3\pi_u)$, followed by $(6\sigma_u)$, $(7\sigma_g)$ and Rydberg orbitals [27]. The energy values of the absorption resonances obtained in our measurements are consistently 0.4 eV below the values reported in Ref. [27], which may be related to the energy calibration uncertainties in the two measurements.
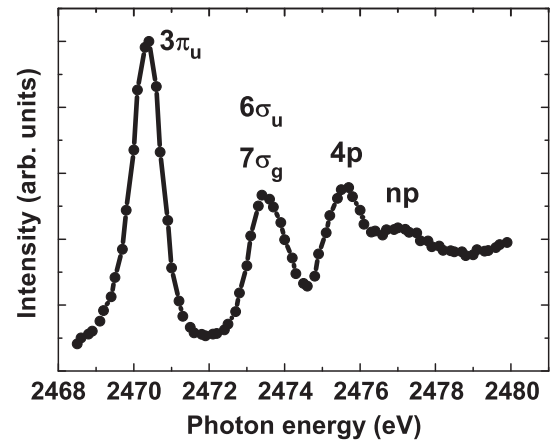
FIG. 1. Experimental partial x-ray fluorescence yield of the sulfur K hole in the CS_2 molecule, constructed by integration of the S K_β emission spectrum over the 2445–2485 eV energy range, at fixed incidence photon energy. The emission spectra are recorded at the scattering angle $\theta = \pi/2$, in the direction of the incident polarization. The absorption resonances are assigned according to [27] as transitions from the S 1s shell to the LUMO $(3\pi_u)$, followed by $(6\sigma_u)$, $(7\sigma_g)$, and Rydberg orbitals.

A series of RIXS S K_β spectra were acquired near the S 1s → $3\pi_u$ LUMO resonance (centered at 2470.4-eV photon energy), with a total instrumental resolution of about 0.27 eV HWHM determined from the measured elastic peak. The RIXS spectra are shown in Fig. 2 as a function of energy loss, corresponding to the difference between the scattered and the incident photon energy. The values of the incident photon-energy detuning Ω from the LUMO resonance are shown in the panels. At $\Omega = -1.9$ eV and -10 eV, the pressure of CS₂ vapor was increased up to 300 mbar in order to compensate for the drop in the signal intensity. One can observe a strong evolution of the RIXS spectral shape with the photon-energy detuning around the first absorption resonance. At positive detuning values, when the photon energy is set above the resonant LUMO excitation energy, the RIXS profile contains contributions from the excitation of higher MOs. At resonance ($\Omega = 0$ eV), the major emission bands,

labeled in Fig. 2 as A, B, and C, can be assigned as transitions to the final states $|2\pi_g^{-1}3\pi_u^1\rangle$, $|2\pi_u^{-1}3\pi_u^1\rangle$, and $|5\sigma_u^{-1}3\pi_u^1\rangle$, respectively, similar to earlier nonresonant fluorescent measurements [27]. Remarkably, the dominant band A corresponds to a symmetry-forbidden transition from the gerade electronic ground state Σ_g^+ to the ungerade final state. Moreover, this symmetry-forbidden peak remains dominant in all the spectra measured for detuning values down to $\Omega = -10$ eV below resonance.

Evolution of the RIXS profile towards large negative detuning values ($\Omega = -10$ eV) reveals a significant relative enhancement of the B and C emission bands as well as the appearance of additional transitions at the low-energy tail of the RIXS spectrum. The goal of our study is to reveal the physical origin of the observed unexpected dependence of the RIXS profile on the photon-energy detuning Ω and to elucidate the mechanism responsible for the observed symmetry-forbidden transitions.

III. MECHANISM OF SYMMETRY BREAKING IN THE HARD X-RAY REGIME

The dependence of the RIXS profile on the detuning Ω was extensively studied in the soft x-ray region. Here, we point out two cases that are found to be relevant for the validity of the symmetry selection rules and Ω dependence of the scattering.

The first mechanism is related to the parity selection rules in RIXS in homonuclear diatomic molecules [5,7,28,29]. Here, the selection rules establish a direct correspondence between the symmetry of the unoccupied and the occupied states involved in the RIXS process. In this case, the shape of the RIXS spectral profile depends on the symmetry of unoccupied MO resonantly populated by absorption of a photon with a given energy.

The second reason for RIXS dependence on Ω is the breakdown of the Born-Oppenheimer approximation in polyatomic molecules with an element of symmetry. Asymmetric vibrations couple the quasidegenerated core-excited states of opposite parity, which leads to the localization of the core hole on one of the equivalent atoms. This dynamic symmetry breaking (DSB) was theoretically predicted [30] and experimentally observed in the soft x-ray regime using photoelectron spectroscopy [31,32] and RIXS [33–35]. The strength of DSB depends on the interplay of the vibrational period and the scattering duration of the RIXS process [8,9,33]. Thus, the dependence of the RIXS duration on the photon-energy detuning provides an efficient tool to actively manipulate the symmetry breaking and its restoration. The DSB is most efficient near resonance, where the RIXS duration is at its maximum determined by the natural lifetime of the core-excited state. Detuning the photon energy away from resonance makes the RIXS duration significantly shorter than the vibrational period. This quenches DSB and leads to symmetry restoration. Therefore, the fingerprint of DSB consists of quenching of
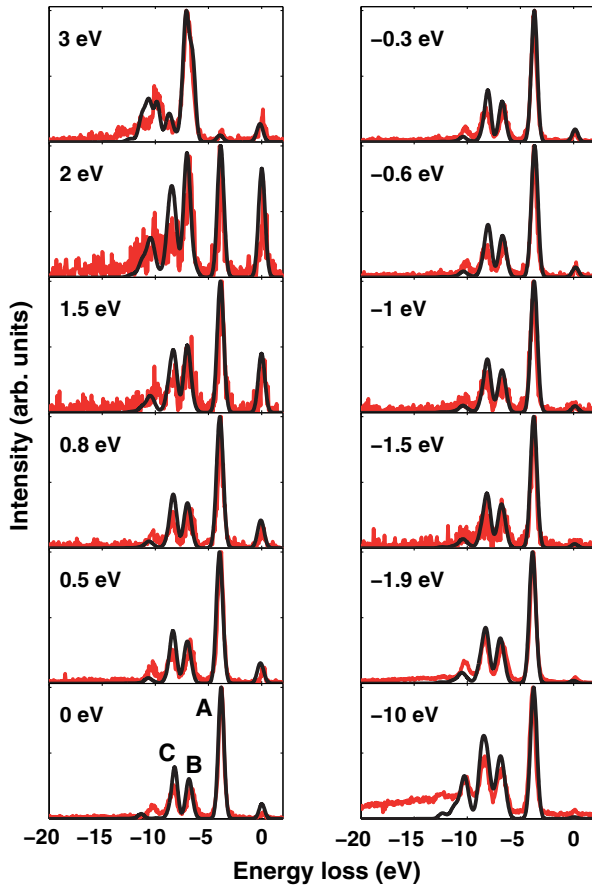
FIG. 2. Experimental (red line) and calculated (black line) S K_β RIXS spectra of the CS₂ molecule for different values of the incident photon-energy detuning Ω from the $1s \to 3\pi_u$ LUMO resonance. At the $3\pi_u$ resonance (2470.4-eV photon energy, $\Omega = 0$ eV), the major emission bands labeled as A, B, and C are assigned as transitions to the final states $|2\pi_g^{-1}3\pi_u^1\rangle$, $|2\pi_u^{-1}3\pi_u^1\rangle$, and $|5\sigma_u^{-1}3\pi_u^1\rangle$, respectively. The error bars on the peak intensities reflect the experimental statistical error.

the symmetry-forbidden transitions in the RIXS spectrum with the photon-energy detuning.

Although the mechanisms considered above are relevant in the soft x-ray regime, neither of them is applicable to our hard x-ray S K_β RIXS spectra in the CS_2 molecule measured for the scattering angle $\theta = \pi/2$. First, in the short-wavelength region, except for the case of small-angle scattering, the parity selection rules are strongly violated because of the quenching of the Young's double-slit (YDS) interference, simply because the x-ray wavelength is shorter than the internuclear distance [5,7,36–38]. Therefore, the first mechanism discussed above cannot be the reason for the observed Ω dependence of the CS_2 RIXS profile. Because of the violation of the symmetry selection rules, DSB also becomes irrelevant in our case. This can explain why our experiment does not display the main fingerprint of DSB—the efficient quenching of the symmetry-forbidden peak with the detuning.

Let us now demonstrate that in the hard x-ray regime, the reason for the strong violation of the symmetry selection rules in CS_2 is the suppression of YDS interference of the waves scattering on the equivalent sulfur atoms. In analogy to the YDS diffraction experiment, illustrated in Fig. 3, the interference depends on the ratio between the wavelength of the scattering light and the distance between the scattering centers. In this case, the core holes localized on the sulfur atoms play the role of the slits for the scattering waves. In the following, we show that the dependence of the interference term in the scattering cross section on the spatial orientation of the molecular axis leads to the orientational dephasing of YDS patterns measured in an ensemble of randomly oriented molecules. The resulting suppression of YDS interference leads to a complete

FIG. 3. Schematic showing an analogy between the RIXS process in CS_2 and the Young double-slit diffraction experiment, where the role of the slits is played by the sulfur atoms serving as the scattering centers. Dynamic symmetry breaking due to asymmetric stretching vibrations in the CS_2 molecule plays only a minor role in our case and does not affect the RIXS profile.

decoherence of the RIXS channels involving the localized core holes and, hence, to a strong violation of the selection rules [7,36]. This happens in a wide range of scattering angles, except for small-angle scattering, where the YDS interference reaches a maximum and the DSB plays a dominant role in the violation of the selection rules.

The starting point of the theoretical analysis is based on the Kramers-Heisenberg formula for the scattering amplitude [39] in the hard x-ray region [7]. The question of whether a core hole should be localized or delocalized is a fundamental problem in x-ray spectroscopy which up to now remains topical [40]. There are numerical (or quantum chemical) and physical aspects behind this classical problem (see Appendix A). Essentially, both localized and delocalized core-excited states are equivalent as long as one ignores a small splitting between gerade and ungerade core-excited states [7,8]. Here, we use the localized picture, which is numerically simpler and provides a direct link to the fundamental physical phenomenon—YDS interference. To restore the symmetry of a quantum system, broken in a localized representation, the RIXS amplitude should be presented as a sum of the partial scattering amplitudes through the core-excited states localized on the left and right sulfur atoms [7,8] (we use atomic units):

$$F = F_1 e^{-\imath \mathbf{q} \cdot \mathbf{R}_1} \pm F_2 e^{-\imath \mathbf{q} \cdot \mathbf{R}_2},$$

$$\mathbf{q} = \mathbf{k}' - \mathbf{k}, \qquad q = 2k \sin\frac{\theta}{2}, \qquad \theta = \angle(\mathbf{k}', \mathbf{k}), \qquad (1)$$

where $+$ and $-$ correspond to the gerade and ungerade final states, respectively. In this process, the frequency ω', polarization $\mathbf{e}'$, and momentum $\mathbf{k}'$ of the scattered photon differ from ω, $\mathbf{e}$, and $\mathbf{k}$ of the incident photon. The partial scattering amplitude

$$F_n = (\mathbf{e}' \cdot \mathbf{d}_{fc})(\mathbf{e} \cdot \mathbf{d}_{c0}) \sum_{\nu_n} \frac{1}{Z_\nu} \langle \nu_f | \nu_n \rangle \langle \nu_n | 0 \rangle, \qquad (2)$$

describes the scattering through the core-hole state localized on the nth sulfur atom ($n = 1, 2$). The labels 0, c, and f mark the ground, intermediate, and final electronic states, respectively. Here, $\mathbf{d}_{c0}$ and $\mathbf{d}_{fc}$ are the electronic-transition dipole moments of the core excitation and emission transitions, respectively. The Franck-Condon amplitudes for the asymmetric stretching mode are denoted as $\langle \nu_f | \nu_n \rangle$ and $\langle \nu_n | 0 \rangle$, where $|0\rangle$, $|\nu_n\rangle$, and $|\nu_f\rangle$ are the lowest vibrational state of the ground state, of the core-excited state with the core hole localized on the nth sulfur atom, and of the final state, respectively; $Z_\nu = \omega - \omega_{c0} + (\varepsilon_\nu - \varepsilon_0) + \imath \Gamma$; $\omega_{ij} = E_i - E_j$ is the adiabatic transition energy of the electron transition $i \to j$; ε_ν is the energy of the νth vibrational level of the asymmetric stretching mode. The lifetime broadening for the S 1s core hole is $\Gamma \approx 0.26$ eV (HWHM) [41].
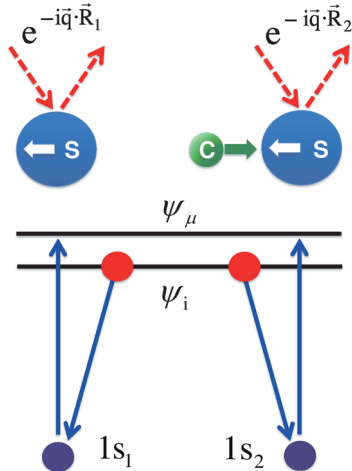
The expression for the scattering cross section $\sigma = \overline{|F|^2} = |F_1|^2 + |F_2|^2 \pm 2\text{Re}(F_1^* F_2 e^{i\mathbf{q}\cdot\mathbf{R}})$ contains the interference contribution

$$\sigma_{\text{int}} = \overline{2\text{Re}(F_1^* F_2 e^{i\mathbf{q}\cdot\mathbf{R}})} \propto \overline{\cos(\mathbf{q}\cdot\mathbf{R})}, \qquad (3)$$

where $\mathbf{R} = \mathbf{R}_1 - \mathbf{R}_2$ is the radius vector between the sulfur atoms and the overline shows the averaging over molecular orientations. This contribution modifies the parity selection rules when the molecules are fixed in space [42]. The collection of RIXS photons from randomly oriented molecules with different orientations of $\mathbf{R}$ results in a suppression of the averaged σ_{int} due to its orientational dephasing: $\sigma_{\text{int}} \propto \overline{\cos(\mathbf{q}\cdot\mathbf{R})} = \sin(qR)/qR \to 0$, when $qR \gg 1$.

To illustrate this point, let us consider the case of LUMO $1s \to 3\pi_u$ resonant excitation. The ratio of the integral scattering cross sections to the final symmetry-forbidden ungerade $f = u = |2\pi_g^{-1} 3\pi_u\rangle$ and the symmetry-allowed gerade $f = g = |2\pi_u^{-1} 3\pi_u\rangle$ states is

$$\frac{\sigma_{2\pi_g}}{\sigma_{2\pi_u}} = \frac{d_{2\pi_g 1s}^2}{d_{2\pi_u 1s}^2}\left(\frac{1-\rho}{1+\rho}\right), \qquad (4)$$

where the interference term $\rho = \sigma_{\text{int}}/(\overline{|F_1|^2 + |F_2|^2})$, in general, includes both the YDS (ρ_{yds}) and the vibronic coupling [$\rho_{\text{vib}}(\Omega)$] [43] effects

$$\rho = \rho_{\text{yds}}\rho_{\text{vib}}(\Omega),$$

$$\rho_{\text{vib}}(\Omega) = \frac{2\text{Re}\left(\sum_{\nu_1,\nu_2}\frac{\langle 0|\nu_1\rangle\langle\nu_1|\nu_2\rangle\langle\nu_2|0\rangle}{Z_{\nu_1}Z_{\nu_2}^*}\right)}{\sum_{n=1,2}\sum_{\nu_n}\frac{|\langle\nu_n|0\rangle|^2}{|Z_{\nu_n}|^2}}. \qquad (5)$$

Here, $|\rho_{\text{vib}}(\Omega)| \leq 1$ and $\rho_{\text{vib}}(\Omega) \to 1$ when $|\Omega| \gg \varepsilon_0$.

The conservation of the symmetry selection rules with a suppression of the symmetry-forbidden transition [$\sigma_{2\pi_g} = 0$ in Eq. (4)] is fulfilled only when the interference term is equal to 1: $\rho = 1$. In our experiment ($\mathbf{e}' \perp \mathbf{e}$, $\theta = \pi/2$), the selection rules are violated because of a small negative value of the YDS factor, $\rho_{\text{yds}} \approx -0.16$ [7,36]. This value of ρ_{yds} can be easily obtained using the equation (see Appendix B for the derivation)

$$\rho_{\text{yds}} = \frac{5}{2}\left[j_0(Q) - 2\frac{j_1(Q)}{Q} + j_2(Q)\left(\cos^2\frac{\theta}{2} + \frac{1}{Q^2}\right)\right. $$
$$\left. - \frac{j_3(Q)}{Q}\cos^2\frac{\theta}{2}\right], \qquad (6)$$

which is valid for $\mathbf{e}' \perp \mathbf{e}$ and an arbitrary scattering angle θ. Here, $j_l(Q)$ are the spherical Bessel functions, $Q = qR = 2kR\sin(\theta/2)$, $k = 0.663$ a.u., $R = 5.9$ a.u. is the distance between the two sulfur atoms. Note that the YDS factor ρ_{yds} [see Eq. (6)] differs from $\overline{\cos(\mathbf{q}\cdot\mathbf{R})} = j_0(Q) = \sin(Q)/Q$ because of the anisotropic prefactor $(\mathbf{e}'\cdot\mathbf{d}_{fc})(\mathbf{e}\cdot\mathbf{d}_{c0})$ in the RIXS amplitude [Eq. (2)].

The DSB effect due to asymmetric stretching vibrations in the CS$_2$ molecule (Fig. 3), described by $\rho_{\text{vib}}(\Omega)$, plays only a minor role in our experiment because of the smallness of the YDS factor ρ_{yds}. Therefore, the dependence of the RIXS profile on the photon-energy detuning Ω, typical for DSB [33,34], is irrelevant to our experiment.

Importantly, the mechanism of symmetry breaking, due to the orientational dephasing of YDS interference in randomly oriented molecules, is specific to the hard x-ray regime [5–8,44,45]. The YDS mechanism remains dominant in the hard x-ray regime, except for the small-angle scattering, where $\theta \lesssim 15^0$, $qR \approx kR\theta < 1$, and $\rho_{\text{yds}} \approx 1$, so that YDS dephasing is absent and the DSB mechanism begins playing the dominant role [see Eq. (6) and Fig. 4]. Therefore, both qualitatively different mechanisms of the symmetry rules violation, YDS and DSB, can be potentially observed in a CS$_2$ molecule in the hard x-ray RIXS experiment under the conditions of large-angle ($\theta = \pi/2$) and small-angle ($\theta \lesssim 15^0$) scattering, respectively.

Contrary to the hard x-ray regime, in the soft x-ray regime, where $qR \ll 1$, YDS dephasing is absent for any scattering angle, and the selection rules can be broken only due to the localization of a core hole in the course of asymmetric stretching vibrations $\rho \to \rho_{\text{vib}}$, as previously observed for the CO$_2$ molecule [33,34].

We would like to point out that the breakdown of the selection rules caused by YDS interference [7,37] can be alternatively interpreted in terms of a nondipole effect [36,38] because, in our case, the size of the system is larger than the photon wavelength, thus justifying violation of the selection rules.
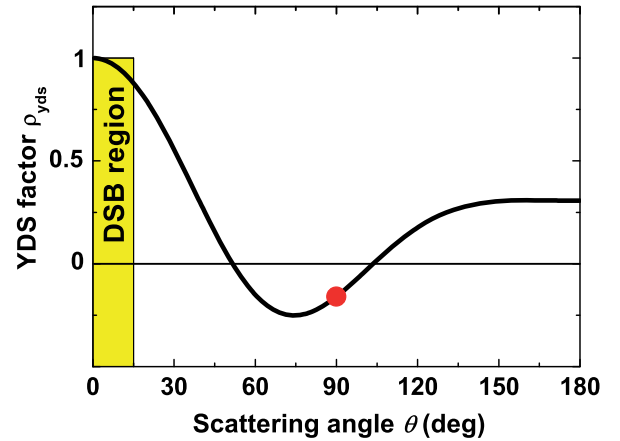

FIG. 4. The dependence of the YDS factor ρ_{yds} [Eq. (6)] on the scattering angle $\theta = \angle(\mathbf{k}',\mathbf{k})$ for S K_β RIXS of CS$_2$ with $\mathbf{e}' \perp \mathbf{e}$. The DSB mechanism is responsible for the breakdown of selection rules at the small-angle scattering (shaded area), where $\rho_{\text{yds}} \approx 1$. This is in contrast to large-angle scattering, where $\rho_{\text{yds}} \ll 1$ and the reason for the selection-rules violation is the orientational dephasing of YDS interference. Our experiment was performed at $\theta = \pi/2$, where $\rho_{\text{yds}}(\pi/2) \approx -0.16$ (circle) and the YDS interference is absent, which leads to violation of the selection rules.

The insight obtained into the mechanism of symmetry breaking in CS_2 excited at the S 1s shell under the experimental conditions with $\theta = \pi/2$ allows us to make important assumptions in our numerical simulations outlined hereafter.

IV. OUTLINE OF THE NUMERICAL SIMULATIONS

Because of a strong suppression of YDS interference, as shown in the previous section, our simulations considered core-excited states $|c\rangle$ with a localized core hole. The vibrational structure was neglected because, in the absence of the DSB effect, the only consequence of vibrations is the broadening of the spectral lines. The RIXS cross section of randomly oriented CS_2 molecules was computed using the standard Kramers-Heisenberg equation [8,39]

$$\sigma(\omega', \omega) = \omega\omega'^3 \sum_f \overline{|F_f|^2} \, \Phi(\omega' - \omega + \omega_{f0}),$$

$$F_f = \sum_c \frac{(\mathbf{e}' \cdot \mathbf{d}_{fc})(\mathbf{e} \cdot \mathbf{d}_{c0})}{\omega - \omega_{c0} + i\Gamma}. \tag{7}$$

The orientational averaging of the RIXS cross section $\sigma(\omega', \omega)$ was performed similarly to Refs. [7,8,46]. The spectral function of the incident radiation was modeled by the Gaussian $\Phi(\Omega) = \exp(-\Omega^2 4 \ln 2/\gamma^2)$ with $\gamma = 0.4$ eV, corresponding to the experimental photon bandwidth.

Our *ab initio* calculations are performed using the configuration interaction (CI) method. The CI active space contains the eight highest occupied MOs, the 50 lowest intermediate core-excited states, and the 100 lowest final valence-excited states. In the ground state, the linear CS_2 molecule belongs to the $D_{\infty h}$ symmetry group, which is also used in our calculations to describe the final valence-excited states. However, in the intermediate core-excited states, the calculations consider the S 1s core hole localized on one of the sulfur atoms, which breaks the symmetry in the molecule and imposes the use of the $C_{\infty v}$ symmetry group. The initial ground state, the core-excited intermediate states at the sulfur K edge, and the excited valence final states are built using an original approach relying on a set of restricted open-shell Hartree-Fock–self-consistent-field (ROHF-SCF) orthogonal MOs optimized for a singly core-ionized molecular ion. This optimization is realized from a usual 6-311G atomic basis set complemented by the $(3s, 3p, 3d)$ diffuse orbitals in order to better describe relaxation of the valence orbitals in the presence of a localized S 1s core hole.

Afterwards, using this unique set, a post Hartree-Fock configuration interaction (CI-SD) procedure is implemented to simultaneously describe the ground state of the neutral molecule, the single core-excited states, and the valence-excited final states. This CI procedure is performed in the $C_{\infty v}$ symmetry group. Simulations of the RIXS spectra

required computation at the CI-SD level of the theory of the electronic-dipole-transition moments between the neutral ground state and the core-excited electronic states, as well as the transition moments between the intermediate core-excited states and the final states of interest.

The results of our calculations are shown in Fig. 2. The computed and the experimental spectra are superimposed and normalized to the intensity of the dominant peak. Good agreement for peaks A and B confirms the validity of our assumption about the core-hole localization and encourages performing further detailed analyses. A limited number of intermediate and final electronic states involved in the calculations results in a relatively worse agreement for peak C. This is, however, not critical for the rest of the discussion, which is essentially focused on the origin of dominant peak A. Our calculations allow us to extract the symmetry of the final states contributing to emission band A resulting from the decay transition $2\pi_g \to 1s$ upon the resonant LUMO excitation $1s \to 3\pi_u$. Figure 5 shows the calculated resonant RIXS spectrum presented in Fig. 2 at $\Omega = 0$. The dominant emission band A contains two final states $|2\pi_g^{-1}3\pi_u^1\rangle$ of Σ_u^- and Δ_u symmetries at the energy loss values of 3.8 eV and 3.9 eV, respectively. Both of these ungerade final states correspond to symmetry-forbidden transitions and were previously observed around 3.9–4.0 eV using electron energy-loss [47] and optical [48] spectroscopy in the ultraviolet energy range.

As we have shown in Sec. III, the reason for the appearance of the symmetry-forbidden final states in the RIXS profile is the orientational dephasing of the YDS interference, which quenches ρ_{yds} in our hard x-ray experiment with orthogonal scattering geometry ($\theta = \pi/2$). The situation is qualitatively different for small-angle scattering, where $\rho_{yds} \to 1$ [see Fig. 4 and Eq. (6)]. In this case, the only mechanism of symmetry breaking is due to the DSB
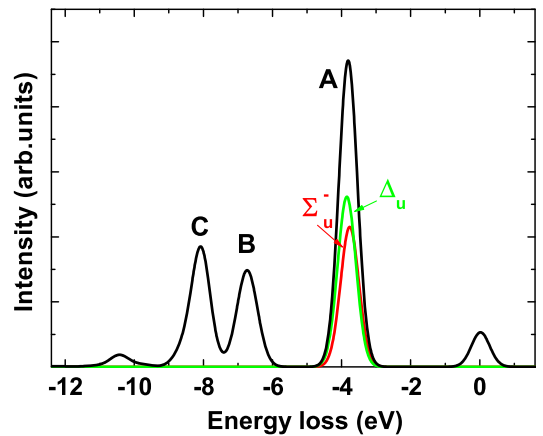

FIG. 5. Calculated S K_β RIXS spectrum of the CS_2 molecule at the $1s \to 3\pi_u$ LUMO resonance (black line), corresponding to the spectrum shown in Fig. 2 at $\Omega = 0$. The arrows show the symmetry-forbidden ungerade final states $|2\pi_g^{-1}3\pi_u^1\rangle$ contributing to the dominant band A.

effect described by the factor $\rho_{\text{vib}}(\Omega)$ [see Eq. (5)], which restores the selection rules [$\rho_{\text{vib}}(\Omega) \rightarrow 1$] for large negative detuning [9].

The good agreement between the numerical simulations and the experimental data gives us an opportunity to reveal the origin of the observed unexpected evolution of the RIXS profile with the excitation photon energy. In the following sections, we discuss two mechanisms responsible for the RIXS excitation-energy dependence in the vicinity of the first absorption resonance ($\Omega \gtrsim -10$ eV) and far from the resonant excitation ($\Omega \rightarrow -\infty$).

V. EVOLUTION OF THE RIXS PROFILE AT SMALL NEGATIVE DETUNING VALUES: SLOW SCATTERING

The mechanism discussed in this section relates the dependence of the RIXS spectra on the photon-energy detuning $\Omega \gtrsim -10$ eV observed in Fig. 2 to the varying partial contributions of the intermediate core-excited states. The *ab initio* calculations, presented above, take into account the involvement of all the intermediate multi-electron core-excited states including the interference effects between them. To give insight into the physical origin of the RIXS Ω dependence, let us consider, in this section, a simplified picture ignoring interference of the intermediate core-excited states. In this case, the RIXS cross section is a sum of the partial cross sections for different core-excited states involving only one of the unoccupied MOs.

Considering a core hole localized on one of the sulfur atoms, RIXS can be presented in the one-electron approximation as the following spectator scattering:

$$|0\rangle \rightarrow |1s^{-1}\psi_\mu\rangle \rightarrow |\psi_i^{-1}\psi_\mu\rangle. \quad (8)$$

The absorption of a photon ω is accompanied by the excitation of the S 1s electron into the unoccupied MO ψ_μ. Then, the decay of an electron from an occupied MO ψ_i to the S 1s core hole leads to the emission of a photon ω'. This allows one to decompose the RIXS cross section into the absorption and emission parts,

$$\sigma(\omega',\omega) = \sum_i^{\text{occ}} \sum_\mu^{\text{unocc}} \overline{(\mathbf{e} \cdot \mathbf{d}_{1s\psi_\mu})^2 (\mathbf{e}' \cdot \mathbf{d}_{\psi_i 1s}^{(\mu)})^2 \frac{\delta(\omega'-\omega+\omega_{f0})}{(\omega-\omega_{\mu 1s})^2 + \Gamma^2}}$$

$$= \sum_\mu^{\text{unocc}} \sigma_\mu(\omega',\omega),$$

$$\sigma_\mu(\omega',\omega) = \overline{\sigma_\mu^{\text{abs}}(\omega)} \times \overline{\sigma_\mu^{\text{emis}}(\omega'-\Omega_\mu)}, \quad (9)$$

where $\Omega_\mu = \omega - \omega_{\mu 1s}$ is the detuning of the excitation energy from the resonant absorption transition S $1s \rightarrow \psi_\mu$. Here, the absorption and the emission parts read

$$\sigma_\mu^{\text{abs}}(\omega) = \frac{(\mathbf{e} \cdot \mathbf{d}_{1s\psi_\mu})^2}{(\omega - \omega_{\mu 1s})^2 + \Gamma^2},$$

$$\sigma_\mu^{\text{emis}}(\omega'-\Omega_\mu) = \sum_i^{\text{occ}} (\mathbf{e}' \cdot \mathbf{d}_{\psi_i 1s}^{(\mu)})^2 \delta(\omega'-\omega_{i,1s}^{(\mu)}-\Omega_\mu). \quad (10)$$

According to Eq. (9), the total RIXS profile is a sum of the partial emission bands $\sigma_\mu^{\text{emis}}(\omega'-\Omega_\mu)$ weighted by the partial absorption cross section $\sigma_\mu^{\text{abs}}(\omega)$ and shifted by the energy spacing $\Delta E_\mu = \omega_{\mu 1s} - \omega_{3\pi_u 1s}$ between the μth unoccupied MO and LUMO $3\pi_u$. The variation of the weights $\sigma_\mu^{\text{abs}}(\omega)$ of the shifted partial emission profiles $\sigma_\mu^{\text{emis}}(\omega'-\Omega_\mu)$ with the photon energy ω explains the Ω dependence of the RIXS shape. The promotion of an excited electron into the unoccupied MO ψ_μ affects the transition dipole moments $\mathbf{d}_{\psi_i 1s}^{(\mu)}$ and the transition energies $\omega_{i,1s}^{(\mu)}$ for the emission transitions $\psi_i \rightarrow$ S 1s. Consequently, the partial emission profiles are not only shifted but also have different spectral shapes.

Let us illustrate this general mechanism of the RIXS formation for the CS$_2$ molecule studied, taking into account two lowest core-excited states, $|1s^{-1}3\pi_u\rangle$ and $|1s^{-1}6\sigma_u\rangle/|1s^{-1}7\sigma_g\rangle$. The corresponding partial cross sections are shown in Fig. 6. As a reference, the total RIXS spectrum, including multielectron and interference effects, is shown. At the resonance, when $\Omega_\mu \equiv \Omega_{3\pi_u} = \omega - \omega_{3\pi_u 1s} = 0$, the RIXS profile is almost entirely given by the $|1s^{-1}3\pi_u\rangle$ intermediate state (top panel in Fig. 6).
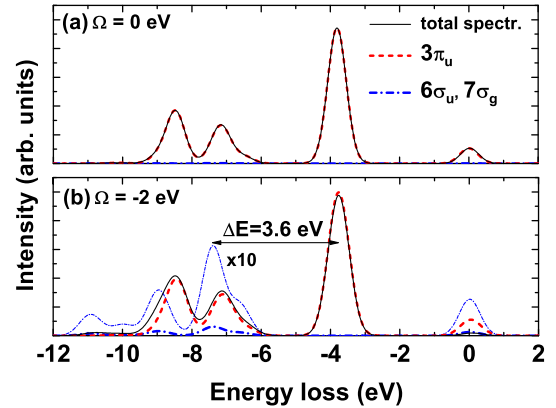
FIG. 6. Partial S K_β RIXS cross sections $\sigma_\mu(\omega,\omega')$ [see Eq. (9)] of the CS$_2$ molecule corresponding to the scattering through the $|1s^{-1}3\pi_u\rangle$ and $|1s^{-1}6\sigma_u/7\sigma_g\rangle$ core-excited states. As a reference, the total RIXS spectrum including multielectron and interference effects is shown as the black solid line. The calculations are performed for the excitation-energy detuning from the $1s \rightarrow 3\pi_u$ LUMO resonance: (a) $\Omega = 0$ and (b) $\Omega = -2$ eV. The thin curve shows the $|1s^{-1}6\sigma_u/7\sigma_g\rangle$ partial contribution with intensity multiplied by 10 for visibility. The partial emission profiles $\sigma_{3\pi_u}^{\text{emis}}$ and $\sigma_{6\sigma_u/7\sigma_g}^{\text{emis}}$ are shifted by $\Delta E \approx 3.6$ eV, the energy spacing between the first two absorption resonances.

Detuning the excitation energy 2 eV below the S $1s \rightarrow 3\pi_u$ resonance (bottom panel in Fig. 6) relatively reduces the weight ($\sigma_{3\pi_u}^{\text{abs}}$) of the dominant channel from the $|1s^{-1}3\pi_u\rangle$ state and gives rise to the contribution from the higher-lying intermediate state $|1s^{-1}6\sigma_u\rangle/|1s^{-1}7\sigma_g\rangle$. These two partial emission profiles $\sigma_{3\pi_u}^{\text{emis}}$ and $\sigma_{6\sigma_u/7\sigma_g}^{\text{emis}}$ are relatively shifted by

$$\Delta E = \omega_{6\sigma_u,7\sigma_g;1s} - \omega_{3\pi_u 1s} \approx 3.6 \text{ eV}, \qquad (11)$$

which is the energy spacing between the first two absorption resonances (see the assignment of the absorption resonances in Fig. 1). The emergence of the $\sigma_{6\sigma_u/7\sigma_g}^{\text{emiss}}$ band explains the deformation of the RIXS profile (Fig. 6) with detuning Ω.

Further detuning of the excitation energy below the LUMO absorption resonance leads to a relative suppression of the LUMO contribution with respect to the emission signal from the higher unoccupied MOs that gives rise to the emission bands in the RIXS profile, redshifted according to the spacing between the corresponding core-excited states. As the excitation energy is lowered, the partial contributions build up the structure in the total RIXS profile at the low-energy side of the dominant emission band as observed in Fig. 2. Note that in the case where both the intermediate and the final states are deep core-hole states, the RIXS spectrum recorded at the excitation energy, strongly detuned below the absorption edge, can serve as reconstruction of the absorption profile [49,50].

The importance of the interference between the intermediate states, neglected in Eqs. (9) and (10), can be revealed through the intensity of the elastic peak (at the zero energy loss) in Fig. 6(b). The sum of the intensities of the elastic peak given by the partial cross sections (red dashed and blue dash-dotted lines) strongly overestimates the intensity of this peak in the total spectrum (black solid line), where the interference is included. The multielectron and interference effects play a crucial role in the mechanism of RIXS Ω dependence dominant at large negative detuning values, which we discuss in the following section.

VI. EVOLUTION OF THE RIXS PROFILE AT LARGE NEGATIVE DETUNING VALUES: FAST SCATTERING

The mechanism described in Sec. V explains the Ω dependence of the RIXS profile until $\Omega \gtrsim -10$ eV. Indeed, the relative weights $\sigma_\mu^{\text{abs}}/\sum_n \sigma_n^{\text{abs}}$ of the partial emission profiles in Eq. (9) cease to vary with Ω for $\Omega < -10$ eV. However, strict multielectron simulations presented in Fig. 7 for Ω up to -500 eV display much slower convergence of the RIXS profile to the limit $\Omega \rightarrow -\infty$. The reason for the RIXS profile evolution at large negative detuning values is the interference of the intermediate core-excited states due to electron correlation. Electronic-state lifetime interferences were previously observed in RIXS spectra of HCl at excitation energies between the two resonances, where the two intermediate states are excited
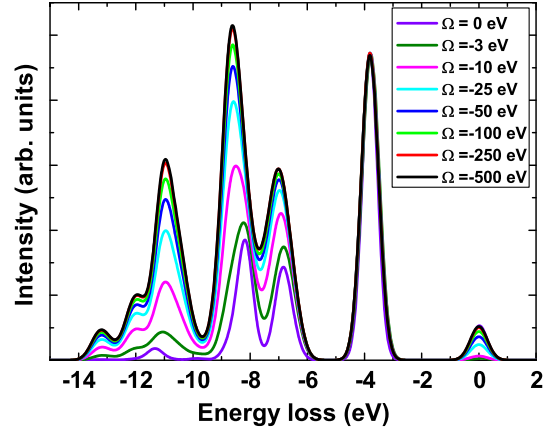

FIG. 7. Calculated S K_β RIXS spectra of the CS_2 molecule for different excitation-energy detuning values below the $1s \rightarrow 3\pi_u$ LUMO resonance. The evolution of the electron wave packet is reflected in the Ω dependence of the RIXS profile for the detuning values larger than the energy spacing between the absorption bands.

with comparable strengths [21]. At the excitation energy tuned significantly below the LUMO resonance, the coherent excitation of all unoccupied MOs occurs with comparable strengths, thus allowing for the interference between all the intermediate multielectron core-excited states.

To shed light on this mechanism, let us consider one of the strongest correlation effects—a relaxation of the electron system in the field of a core hole localized on one of the sulfur atoms [51]. Because of the symmetry breaking in the core-excited state $|c\rangle = |1s^{-1}\tilde{\psi}_{\mu'}\rangle$, the asymmetrical MOs in core-excited state $\tilde{\psi}$ differ from the symmetrical MOs ψ in the final state. The dipole moment of the emission transition $|c\rangle = |1s^{-1}\tilde{\psi}_{\mu'}\rangle \rightarrow |f\rangle = |\psi_i^{-1}\psi_\mu\rangle$ reads

$$\left\langle 1s^{-1}\tilde{\psi}_{\mu'}\Big|\sum_\alpha \mathbf{r}_\alpha\Big|\psi_i^{-1}\psi_\mu\right\rangle \approx \langle\tilde{\psi}_i|\mathbf{r}|1s\rangle\langle\tilde{\psi}_{\mu'}|\psi_\mu\rangle$$
$$- \langle\tilde{\psi}_{\mu'}|\mathbf{r}|1s\rangle\langle\tilde{\psi}_i|\psi_\mu\rangle, \quad (12)$$

where the sum is over the electrons. Equation (12) shows that the relaxation effect opens a two-electron decay channel: (1) a dipole transition $\tilde{\psi}_i \rightarrow 1s$ accompanied by the electron excitation $\tilde{\psi}_{\mu'} \rightarrow \psi_\mu$ and (2) a dipole transition $\tilde{\psi}_{\mu'} \rightarrow 1s$ accompanied by the electron excitation $\tilde{\psi}_i \rightarrow \psi_\mu$. Here, we neglected, for simplicity, the overlap between the valence wave functions and the $1s$ core orbital and took into account only orbitals ($\tilde{\psi}_{\mu'}$, $\tilde{\psi}_i$) and (ψ_μ, $1s$) in the Slater determinants $|1s^{-1}\tilde{\psi}_{\mu'}\rangle$ and $|\psi_i^{-1}\psi_\mu\rangle$, respectively.

The interference of the intermediate electronic states in RIXS is absent in the frozen orbital approximation, when there is no relaxation of the MOs in the presence of a core hole. Indeed, when $\langle\tilde{\psi}_{\mu'}|\psi_\mu\rangle = \delta_{\mu'\mu}$ and $\langle\tilde{\psi}_i|\psi_\mu\rangle = 0$, the final state $|f\rangle = |\psi_i^{-1}\psi_\mu\rangle$ can be reached through only one intermediate state $|1s^{-1}\tilde{\psi}_\mu\rangle$ [Eq. (12)]. The picture changes qualitatively when the relaxation is taken into account:

$\langle \tilde{\psi}_{\mu'} | \psi_{\mu} \rangle \neq \delta_{\mu'\mu}$ and $\langle \tilde{\psi}_i | \psi_{\mu} \rangle \neq 0$. This leads to interference of the intermediate electronic states $|c\rangle = |1s^{-1}\tilde{\psi}_{\mu'}\rangle$, which decay to the same final state $|f\rangle = |\psi_i^{-1}\psi_{\mu}\rangle$ according to Eq. (12).

Importantly, because of the time-energy relation, electronic-state interference in the energy domain leads to attosecond dynamics of the electron wave packet in the time domain [8]. It is known from the field of attosecond science that a coherent excitation of several electronic states in a molecule creates a coherent electron wave packet that will evolve in time [52]. In time-resolved laser experiments, this can be achieved using broadband attosecond pulses. However, in synchrotron experiments, using narrow bandwidth radiation, a coherent superposition of excited electronic states can be created in the hard x-ray regime because of the large lifetime broadenings enhancing the overlap of the deep core-excited states [21].

The time scale of electron and nuclear dynamics is connected by the laws of quantum mechanics to the energy spacing between the stationary excited states. For example, the energy spacing of vibrational states on the meV scale is related to the vibrational molecular motion on a time scale of tens to hundreds of femtoseconds. In our case, the absorption of an incident photon in the CS$_2$ molecule creates a coherent superposition of the core-excited states. The energy spacing $\Delta_{c'c}$ between the core-excited electronic states of several eV (see Fig. 1) implies the electron dynamics with a characteristic time $\tau_{\text{el}} \sim 1/|\Delta_{c'c}| \approx 1/|\Delta_{\mu'\mu}|$ of tens of attoseconds.

The RIXS amplitude in the time domain is given by the Fourier transform of the Kramers-Heisenberg scattering amplitude [8,9],

$$F_f = \int_0^{\infty} dt F_f(t), \quad F_f(t) = -\imath \langle f | (\mathbf{e}' \cdot \mathbf{d}) | \Psi(t) \rangle. \quad (13)$$

One can see that the time-dependent scattering amplitude $F_f(t)$ is determined by the projection on the final state of the electron wave packet $|\Psi(t)\rangle$, evolving in the core-excited state:

$$|\Psi(t)\rangle = e^{-\imath ht}(\mathbf{d} \cdot \mathbf{e})|0\rangle e^{\imath \Omega t - \Gamma t}. \quad (14)$$

In our case, $h = H - E_{\text{LUMO}}$, where H is the molecular Hamiltonian and E_{LUMO} is the energy of the LUMO core-excited state in CS$_2$; Γ is the S 1s core-hole lifetime broadening and Ω is the detuning of the excitation energy from the LUMO absorption resonance.

Equations (13) and (14) show that the RIXS process is determined by the characteristic time τ_{el} of the evolution of the electron wave packet in the core-excited state $e^{-\imath ht}(\mathbf{d} \cdot \mathbf{e})|0\rangle$ and by the scattering duration time T [9],

$$\tau_{\text{el}} \sim \frac{1}{|\Delta_{c'c}|}, \qquad T = \frac{1}{\sqrt{\Omega^2 + \Gamma^2}}. \quad (15)$$

Two qualitatively different times characterize the scattering duration: the core-hole lifetime $1/\Gamma$, which is responsible for the irreversible decay of the core-excited state, and the inverse detuning $1/\Omega$, which describes a reversible dephasing of the scattering amplitude $F_f(t)$ in the time domain.

Taking into account the condition of completeness $\sum_c |c\rangle\langle c| = 1$, one can present the electron wave packet [Eq. (14)] as a coherent superposition of multielectron core-excited states $|c\rangle$,

$$|\Psi(t)\rangle = \sum_c \zeta_c |c\rangle e^{\imath \Omega_c t - \Gamma t} \rightarrow \sum_{\mu}^{\text{unocc}} \zeta_{\mu} |1s^{-1}\tilde{\psi}_{\mu}\rangle e^{\imath \Omega_{\mu} t - \Gamma t}. \quad (16)$$

Here, $\zeta_c = (\mathbf{d}_{oc} \cdot \mathbf{e}) \approx \zeta_{\mu} = (\mathbf{d}_{\tilde{\psi}_{\mu}1s} \cdot \mathbf{e})$ is the probability amplitude of the core-excited state $|c\rangle$.

Control over the excitation-energy detuning provides us with a tool to manipulate the dynamics of the electron wave packet, which will be reflected in the RIXS profile. First, let us consider the limiting cases of near-resonant and strongly detuned excitation energy. For the photon energy tuned close to the resonant excitation, where $|\Omega| \sim |\Delta_{c'c}| \sim 10$ eV, the electron wave-packet dynamics affects the RIXS profile. However, the main reason for the RIXS Ω dependence for small detuning values is not related to the interference, as was explained in Sec. V.

When the excitation energy is tuned far below the LUMO resonance, the contributions from all intermediate core-excited states in Eq. (16) experience strong oscillations. These fast sign-changing oscillations of $F_f(t)$ quench the large time contributions $(t > T)$ in the integral [Eq. (13)]. As $|\Omega|$ increases, the scattering duration becomes shorter than the characteristic time of the evolution of the electron wave packet $T \ll \tau_{\text{el}}$, and the scattering amplitude F_f gradually approaches the limit of fast scattering,

$$F_f = \frac{\langle f | (\mathbf{e}' \cdot \mathbf{d}) | \Psi(0) \rangle}{\Omega} = \frac{\langle f | (\mathbf{e}' \cdot \mathbf{d})(\mathbf{e} \cdot \mathbf{d}) | 0 \rangle}{\Omega},$$

$$\Psi(0) = \sum_c \zeta_c |c\rangle = (\mathbf{d} \cdot \mathbf{e})|0\rangle. \quad (17)$$

In this limit of "fast RIXS," the molecule experiences an instantaneous quadrupole transition from the ground to the final state. According to the simulations presented in Fig. 7, the RIXS profile shows a rather slow convergence to the limit of fast scattering (17).

The limiting cases considered set the scene for the discussion of our main finding. We observe an interesting scenario of the RIXS profile evolution with the excitation-energy detuning Ω. When the detuning is small, $|\Omega| \lesssim 10$ eV, the main reason for the dependence on the detuning is the variation of the relative weights of the shifted partial emission bands corresponding to core excitation to different unoccupied MOs. For further detuning down to $\Omega = -500$ eV, our model predicts a growing contribution of coherently excited multielectron core-hole states to the

scattering amplitude. Coherent excitation of these states enables electron dynamics on the time scale $\tau_{el} \sim 1/|\Delta_{c'c}| \lesssim 0.1$ fs. In this regime, the spectral shape of RIXS is determined by the interplay of the scattering duration T and the characteristic time τ_{el} of the electron wave-packet evolution. The calculations presented in Fig. 7 show that the convergence of the RIXS spectrum to the limit of fast scattering [Eq. (17)] occurs for detuning $\Omega \approx -100$ eV, where the scattering duration falls below 10 attoseconds. Further detuning of the excitation energy does not affect the RIXS profile, and the scattering can be considered as instantaneous.

VII. CONCLUSION

Our experimental and theoretical study of the RIXS S K_β spectra in CS_2 has brought us to the following main conclusions.

First, we have elucidated the mechanism responsible for the symmetry-forbidden transitions dominating the RIXS spectra. Violation of the symmetry selection rules occurs because of localization of the S 1s core hole in CS_2 during the RIXS process. The reason for the core-hole localization is the orientational dephasing of YDS interference patterns measured in randomly oriented molecules, which is specific to the hard x-ray regime.

Second, a strong evolution of the RIXS profile with the excitation energy tuned down to about 10 eV below the LUMO resonance is caused by a relative variation of the partial contributions from the different intermediate core-excited states.

Finally, the temporal evolution of the multielectron wave packet launched by a coherent excitation of multiple electronic states is responsible for the excitation-energy dependence of RIXS upon further detuning. Electron dynamics occurs on the characteristic time scale in the attosecond range, determined by the spacing of the coherently excited intermediate states. The RIXS profile is determined by the interplay of the effective scattering duration and the characteristic time of the electron wave-packet evolution. For the scattering duration around 10 as, corresponding to the detuning of around -100 eV, the RIXS profile converges to the limit of fast scattering.

Direct time-resolved measurements of electron dynamics in core-excited molecules require using a short hard x-ray pulse with duration below the core-hole lifetime (around 1 fs), which is unavailable so far. Our study demonstrates the potential of RIXS and core-hole spectroscopy in general, as a promising alternative in the application to the studies of electron dynamics in molecules excited at the deep core shells.

APPENDIX A: LOCALIZED VERSUS DELOCALIZED CORE HOLES

One can alternatively describe core-excited states of CS_2 by either using a delocalized core-hole picture or considering a core hole localized on the left or right sulfur atoms,

$$\text{loc:} \quad |1s_1^{-1}\psi_\mu\rangle, \qquad |1s_2^{-1}\psi_\mu\rangle,$$

$$\text{deloc:} \quad |1\sigma_g^{-1}\psi_\mu\rangle, \qquad |1\sigma_u^{-1}\psi_\mu\rangle. \qquad (A1)$$

As long as a very small splitting between $1\sigma_g \approx (1s_1 + 1s_2)/\sqrt{2}$ and $1\sigma_u \approx (1s_1 - 1s_2)/\sqrt{2}$ core levels can be neglected, both the localized and delocalized representations become equivalent [7,8]. To restore the symmetry of a quantum system, broken in a localized representation, the RIXS amplitude should be written as a sum of the partial scattering amplitudes through the core-excited states localized on the left and right atoms [see Eq. (1)] [7,8].

In spite of the equivalence of both representations (A1), the localized picture has two advantages. The first one has a numerical, or quantum chemical, aspect, demonstrated by Bagus and Schaefer [51], who obtained a more accurate value of the O 1s ionization potential in the O_2 molecule using a localized single-determinant state. They restored the symmetry of the molecule using linear combinations of the localized states. One has to use multiple configurations to reach the same numerical accuracy using delocalized core holes [51]. The second advantage of localized core-excited states is a clearer physical interpretation of the scattering in relation to a fundamental physical phenomenon of YDS interference. Both of these aspects encourage us to use the symmetry-broken localized representation of core-excited states.

APPENDIX B: AVERAGING OVER MOLECULAR ORIENTATIONS

In order to derive the expression for the YDS factor ρ_{yds} [Eq. (6)], the RIXS cross section (7) should be averaged over molecular orientations,

$$\sigma = \sigma_{dir} \pm \sigma_{int}$$

$$\propto \sum_{cc_1} \frac{\overline{(\mathbf{e}' \cdot \hat{\mathbf{d}}_{fc})(\mathbf{e} \cdot \hat{\mathbf{d}}_{c0})(\mathbf{e}' \cdot \hat{\mathbf{d}}_{fc_1})(\mathbf{e} \cdot \hat{\mathbf{d}}_{c_10})(1 \pm \cos(\mathbf{q} \cdot \mathbf{R}))}}{Z_{c_10}^* Z_{c0}},$$

$$\sigma = \sigma_{dir}(1 \pm \rho_{yds}), \qquad \rho_{yds} = \frac{\sigma_{int}}{\sigma_{dir}}, \qquad (B1)$$

where $Z_{c0} = \omega - \omega_{c0} + \iota\Gamma$, and the second term $\sigma_{\text{int}} = \overline{\cdots \cos(\mathbf{q} \cdot \mathbf{R})}$ describes the YDS interference. The overline means the orientational averaging, and $\hat{\mathbf{d}} = \mathbf{d}/d$ is the unit vector along the transition dipole moment $\mathbf{d}$. The summation is over all core-excited states $|c\rangle$ with the core

hole localized on one of the sulfur atoms. Here, we ignore the vibrational degrees of freedom to avoid cumbersome notations, and so $\rho \to \rho_{\text{yds}}$.

The polarization dependence of the direct term σ_{dir} is taken into account explicitly [7] using the following equation:

$$\overline{(\mathbf{e}' \cdot \hat{\mathbf{d}}_{fc})(\mathbf{e} \cdot \hat{\mathbf{d}}_{c0})(\mathbf{e}' \cdot \hat{\mathbf{d}}_{fc_1})(\mathbf{e} \cdot \hat{\mathbf{d}}_{c_10})} = \frac{1}{30}[2(2 - (\mathbf{e}' \cdot \mathbf{e})^2)(\hat{\mathbf{d}}_{fc} \cdot \hat{\mathbf{d}}_{fc_1})(\hat{\mathbf{d}}_{c0} \cdot \hat{\mathbf{d}}_{c_10})$$
$$+ (3(\mathbf{e}' \cdot \mathbf{e})^2 - 1)\{(\hat{\mathbf{d}}_{fc} \cdot \hat{\mathbf{d}}_{c0})(\hat{\mathbf{d}}_{fc_1} \cdot \hat{\mathbf{d}}_{c_10}) + (\hat{\mathbf{d}}_{fc} \cdot \hat{\mathbf{d}}_{c_10})(\hat{\mathbf{d}}_{fc_1} \cdot \hat{\mathbf{d}}_{c0})\}]. \quad (B2)$$

This equation shows that the RIXS cross section depends on the angle between polarization vectors and is sensitive to the mutual orientation of the transition dipole moments of core excitation $\mathbf{d}_{c0}$ and decay $\mathbf{d}_{fc}$ (see review [8] and references therein).

Let us outline the main steps of orientation averaging of the YDS interference contribution σ_{int}. The simplest case is the $\sigma\sigma$ RIXS channel ($1s \to \sigma^*$, $\sigma \to 1s$), where both transition dipole moments are oriented along the internuclear radius vector: $\hat{\mathbf{d}}_{fc} = \hat{\mathbf{d}}_{c0} = \hat{\mathbf{R}}$. Here, σ^* and σ are unoccupied and occupied molecular orbitals. Apparently,

$$\sigma_{\text{dir}}^{\sigma\sigma} = \overline{(\mathbf{e}' \cdot \hat{\mathbf{R}})^2(\mathbf{e} \cdot \hat{\mathbf{R}})^2} = \frac{1}{15}(1 + 2(\mathbf{e}' \cdot \mathbf{e})^2),$$

$$\sigma_{\text{int}}^{\sigma\sigma} = \overline{(\mathbf{e}' \cdot \hat{\mathbf{R}})^2(\mathbf{e} \cdot \hat{\mathbf{R}})^2 \cos(\mathbf{q} \cdot \mathbf{R})} = \overline{(\mathbf{e}' \cdot \hat{\mathbf{R}})^2(\mathbf{e} \cdot \hat{\mathbf{R}})^2 e^{\iota \mathbf{Q} \cdot \hat{\mathbf{R}}}}$$

$$= \sum_{\alpha\beta\gamma\delta} e'_\alpha e'_\beta e_\gamma e_\delta \overline{\hat{\mathbf{R}}_\alpha \hat{\mathbf{R}}_\beta \hat{\mathbf{R}}_\gamma \hat{\mathbf{R}}_\delta e^{\iota \mathbf{Q} \cdot \hat{\mathbf{R}}}} = \sum_{\alpha\beta\gamma\delta} e'_\alpha e'_\beta e_\gamma e_\delta \frac{\partial^4}{\partial Q_\alpha \partial Q_\beta \partial Q_\gamma \partial Q_\delta} \overline{e^{\iota \mathbf{Q} \cdot \hat{\mathbf{R}}}}$$

$$= \sum_{\alpha\beta\gamma\delta} e'_\alpha e'_\beta e_\gamma e_\delta \frac{\partial^4 j_0(Q)}{\partial Q_\alpha \partial Q_\beta \partial Q_\gamma \partial Q_\delta} = [1 + 2(\mathbf{e} \cdot \mathbf{e}')^2] \frac{j_2(Q)}{Q^2} - [(\mathbf{e} \cdot \hat{\mathbf{q}})^2 + (\mathbf{e}' \cdot \hat{\mathbf{q}})^2 + 4(\mathbf{e} \cdot \mathbf{e}')(\mathbf{e} \cdot \hat{\mathbf{q}})(\mathbf{e}' \cdot \hat{\mathbf{q}})] \frac{j_3(Q)}{Q}$$

$$+ (\mathbf{e} \cdot \hat{\mathbf{q}})^2(\mathbf{e}' \cdot \hat{\mathbf{q}})^2 j_4(Q), \quad (B3)$$

where $\alpha, \beta, \gamma, \delta = (x, y, z)$, $\mathbf{Q} = \mathbf{q}R$, $(\mathbf{e} \cdot \hat{\mathbf{q}}) = (\mathbf{e} \cdot \mathbf{k}')/q$ and $(\mathbf{e}' \cdot \hat{\mathbf{q}}) = -(\mathbf{e}' \cdot \mathbf{k})/q$. Note that, for brevity, the prefactor $ww'^3\Phi(\omega' - \omega + \omega_{f0})/|Z_{c0}|^2$ is omitted on the right-hand side of expressions for $\sigma_{\text{dir}}^{\sigma\sigma}$ and $\sigma_{\text{int}}^{\sigma\sigma}$. Here, we used Eq. (B2) and the following properties of the spherical Bessel functions:

$$(2n + 1)\frac{dj_n(Q)}{dQ} = nj_{n-1}(Q) - (n + 1)j_{n+1}(Q),$$

$$j_{n+1}(Q) = \frac{2n + 1}{Q}j_n(x) - j_{n-1}(Q). \quad (B4)$$

The substitution of $\sigma_{\text{dir}}^{\sigma\sigma}$ and $\sigma_{\text{int}}^{\sigma\sigma}$ in Eq. (B1) gives the expression for the YDS factor ρ_{yds} for the studied $\sigma\sigma$ RIXS channel.

The results obtained for the $\sigma\sigma$ channel (B3) allow us to also derive an expression for ρ_{yds} for other RIXS channels such as $\pi\sigma$, $\sigma\pi$, and $\pi\pi$. Here, we demonstrate a derivation for the $\pi\pi$ RIXS channel ($1s \to \pi^*$, $\pi \to 1s$), assuming the π_x and π_y molecular orbitals to be fully occupied. Let us choose the frame so that $z\|\mathbf{R}$, $y\|\mathbf{d}_{1s\pi_y} \equiv \mathbf{d}_{\pi_y}$ and $x\|\mathbf{d}_{1s\pi_x} \equiv \mathbf{d}_{\pi_x}$. Taking into account $1 = (\mathbf{e}_z)^2 + (\mathbf{e}_x)^2 + (\mathbf{e}_y)^2$, we obtain the following identities:

$$1 = (\mathbf{e} \cdot \hat{\mathbf{R}})^2 + (\mathbf{e} \cdot \hat{\mathbf{d}}_{\pi_x})^2 + (\mathbf{e} \cdot \hat{\mathbf{d}}_{\pi_y})^2,$$

$$1 = [(\mathbf{e} \cdot \hat{\mathbf{R}})^2 + (\mathbf{e} \cdot \hat{\mathbf{d}}_{\pi_x})^2 + (\mathbf{e} \cdot \hat{\mathbf{d}}_{\pi_y})^2]$$
$$\times [(\mathbf{e}' \cdot \hat{\mathbf{R}})^2 + (\mathbf{e}' \cdot \hat{\mathbf{d}}_{\pi_x})^2 + (\mathbf{e}' \cdot \hat{\mathbf{d}}_{\pi_y})^2]$$
$$= -(\mathbf{e} \cdot \hat{\mathbf{R}})^2(\mathbf{e}' \cdot \hat{\mathbf{R}})^2 + (\mathbf{e} \cdot \hat{\mathbf{R}})^2 + (\mathbf{e}' \cdot \hat{\mathbf{R}})^2$$
$$+ [(\mathbf{e} \cdot \hat{\mathbf{d}}_{\pi_x})^2 + (\mathbf{e} \cdot \hat{\mathbf{d}}_{\pi_y})^2][(\mathbf{e}' \cdot \hat{\mathbf{d}}_{\pi_x})^2 + (\mathbf{e}' \cdot \hat{\mathbf{d}}_{\pi_y})^2].$$
$$(B5)$$

Since

$$[(\mathbf{e} \cdot \hat{\mathbf{d}}_{\pi_x})^2 + (\mathbf{e} \cdot \hat{\mathbf{d}}_{\pi_y})^2][(\mathbf{e}' \cdot \hat{\mathbf{d}}_{\pi_x})^2 + (\mathbf{e}' \cdot \hat{\mathbf{d}}_{\pi_y})^2]$$
$$= 1 + (\mathbf{e} \cdot \hat{\mathbf{R}})^2(\mathbf{e}' \cdot \hat{\mathbf{R}})^2 - (\mathbf{e} \cdot \hat{\mathbf{R}})^2 - (\mathbf{e}' \cdot \hat{\mathbf{R}})^2, \quad (B6)$$

and $\overline{(\mathbf{e} \cdot \hat{\mathbf{d}}_{\pi_y})^2} = 1/3$, one obtains

$$\sigma_{\text{dir}}^{\pi\pi} = \overline{1 + (\mathbf{e} \cdot \hat{\mathbf{R}})^2(\mathbf{e}' \cdot \hat{\mathbf{R}})^2 - (\mathbf{e} \cdot \hat{\mathbf{R}})^2 - (\mathbf{e}' \cdot \hat{\mathbf{R}})^2}$$
$$= \frac{2}{15}(3 + (\mathbf{e}' \cdot \mathbf{e})^2),$$

$$\sigma_{\text{int}}^{\pi\pi} = \overline{\{1 + (\mathbf{e} \cdot \hat{\mathbf{R}})^2(\mathbf{e}' \cdot \hat{\mathbf{R}})^2 - (\mathbf{e} \cdot \hat{\mathbf{R}})^2 - (\mathbf{e}' \cdot \hat{\mathbf{R}})^2\}e^{\iota\mathbf{Q}\cdot\hat{\mathbf{R}}}}.$$
$$(B7)$$

Substituting

$$\langle(\mathbf{e}\cdot\hat{\mathbf{R}})^2 e^{\imath\mathbf{q}\cdot\hat{\mathbf{R}}}\rangle = -\sum_{\alpha\beta}e_\alpha e_\beta \frac{\partial^2}{\partial Q_\alpha \partial Q_\beta}j_0(Q)$$

$$= \frac{j_1(Q)}{Q} - (\mathbf{e}\cdot\hat{\mathbf{q}})^2 j_2(Q), \qquad \text{(B8)}$$

into Eq. (B7) and taking into account Eq. (B3), one can derive general expressions for $\sigma_{\text{int}}^{\pi\pi}$ and ρ_{yds}.

At this stage, we obtain the expression for ρ_{yds} [Eq. (6)] corresponding to our experimental geometry $(\mathbf{e'}\cdot\mathbf{e}) = 0$,

$$\rho_{\text{yds}} = \frac{\sigma_{\text{int}}^{\pi\pi}}{\sigma_{\text{dir}}^{\pi\pi}} = \frac{5}{2}\left[j_0(Q) - 2\frac{j_1(Q)}{Q} + j_2(Q)\left(\cos^2\frac{\theta}{2} + \frac{1}{Q^2}\right)\right.$$
$$\left. - \frac{j_3(Q)}{Q}\cos^2\frac{\theta}{2}\right]. \qquad \text{(B9)}$$

Here, $\theta = \angle(\mathbf{k'},\mathbf{k})$ is the scattering angle and $Q = 2kR\sin(\theta/2)$.

[1] P. Morin and I. Nenner, *Atomic Autoionization Following Very Fast Dissociation of Core-Excited HBr*, Phys. Rev. Lett. **56**, 1913 (1986).

[2] O. Björneholm, A. Nilsson, A. Sandell, B. Hernnäs, and N. Mårtensson, *Determination of Time Scales for Charge-Transfer Screening in Physisorbed Molecules*, Phys. Rev. Lett. **68**, 1892 (1992).

[3] D. W. Lindle, P. L. Cowan, R. E. LaVilla, T. Jach, R. D. Deslattes, B. Karlin, J. A. Sheehy, T. J. Gil, and P. W. Langhoff, *Polarization of Molecular X-Ray Fluorescence*, Phys. Rev. Lett. **60**, 1010 (1988).

[4] S. Svanberg, *Atomic and Molecular Spectroscopy: Basic Aspects and Practical Applications* (Springer-Verlag, Berlin, 2001).

[5] F. Kh. Gel'mukhanov, L. N. Mazalov, and N. A. Shklyaeva, Zh. Eksp. Teor. Fiz. **69**, 1971 (1975) [*An Interference Effect in X-Ray Fluorescence Spectra*, Sov. Phys. JETP **42**, 1001 (1975)].

[6] F. Kh. Gel'mukhanov, L. N. Mazalov, and N. A. Shklyaeva, Zh. Eksp. Teor. Fiz. **71**, 960 (1976) [*Some Features of X-Ray Fluorescence in Metals near the Absorption Threshold*, Sov. Phys. JETP **44**, 504 (1976)].

[7] F. Gel'mukhanov, and H. Ågren, *Resonant Inelastic X-Ray Scattering with Symmetry-Selective Excitation*, Phys. Rev. A **49**, 4378 (1994).

[8] F. Gel'mukhanov and H. Ågren, *Resonant X-ray Raman Scattering*, Phys. Rep. **312**, 87 (1999).

[9] F. Gel'mukhanov, P. Sałek, T. Privalov, and H. Ågren, *Duration of X-Ray Raman Scattering*, Phys. Rev. A **59**, 380 (1999).

[10] O. Björneholm, S. Sundin, S. Svensson, R. R. T. Marinho, A. Naves de Brito, F. Gel'mukhanov, and H. Ågren, *Femtosecond Dissociation of Core-Excited HCl Monitored by Frequency Detuning*, Phys. Rev. Lett. **79**, 3150 (1997).

[11] R. Feifel, F. Burmeister, P. Salek, M. N. Piancastelli, M. Bässler, S. L. Sorensen, C. Miron, H. Wang, I. Hjelte, O. Björneholm, A. Naves de Brito, F. K. Gel'mukhanov, H. Ågren, and S. Svensson, *Observation of a Continuum-Continuum Interference Hole in Ultrafast Dissociating Core-Excited Molecules*, Phys. Rev. Lett. **85**, 3133 (2000).

[12] D. L. Ederer and J. H. McGuire, *Raman Emission by X-Ray Scattering: Proceedings of the Workshop* (World Scientific, Singapore, 1996).

[13] P. A. Brühwiler, O. Karis, and N. Mårtensson, *Charge-Transfer Dynamics Studied Using Resonant Core Spectroscopies*, Rev. Mod. Phys. **74**, 703 (2002).

[14] L. J. P. Ament, M. van Veenendaal, T. P. Devereaux, J. P. Hill, and J. van den Brink, *Resonant Inelastic X-Ray Scattering Studies of Elementary Excitations*, Rev. Mod. Phys. **83**, 705 (2011).

[15] J. Schnadt, P. A. Brühwiler, L. Patthey, J. N. O'Shea, S. Södergren, M. Odelius, R. Ahuja, O. Karis, M. Bässler, P. Persson *et al.*, *Experimental Evidence for Sub-3-fs Charge Transfer from an Aromatic Adsorbate to a Semiconductor*, Nature (London) **418**, 620 (2002).

[16] A. Föhlish, P. Feulner, F. Hennies, A. Fink, D. Menzel, D. Sanchez-Portal, P. M. Echenique, and W. Wurth, *Direct Observation of Electron Dynamics in the Attosecond Domain*, Nature (London) **436**, 373 (2005).

[17] H. Ikeura-Sekiguchi and T. Sekiguchi, *Attosecond Electron Delocalization in the Conduction Band through the Phosphate Backbone of Genomic DNA*, Phys. Rev. Lett. **99**, 228102 (2007).

[18] T. Marchenko, L. Journel, T. Marin, R. Guillemin, S. Carniato, M. Žitnik, K. Bučar, M. Kavčič, A. Mihelič, J. Hoszowska, W. Cao, and M. Simon, *Resonant Inelastic X-Ray Scattering at the Limit of Subfemtosecond Natural Lifetime*, J. Chem. Phys. **134**, 144308 (2011).

[19] M. Simon, L. Journel, R. Guillemin, W. C. Stolte, I. Minkov, F. Gel'mukhanov, P. Sałek, H. Ågren, S. Carniato, R. Taïeb, A. C. Hudson, and D. W. Lindle, *Femtosecond Nuclear Motion of HCl Probed by Resonant X-Ray Raman Scattering in the Cl 1s Region*, Phys. Rev. A **73**, 020706 (2006).

[20] L. Journel, L. El Khoury, T. Marin, R. Guillemin, S. Carniato, A. Avila, R. Delaunay, C. F. Hague, and M. Simon, *Performances of a Bent-Crystal Spectrometer Adapted to Resonant X-Ray Emission Measurements on Gas-Phase Samples*, Rev. Sci. Instrum. **80**, 093105 (2009).

[21] M. Kavčič, M. Žitnik, K. Bučar, A. Mihelič, S. Carniato, L. Journel, R. Guillemin, and M. Simon, *Electronic State Interferences in Resonant X-Ray Emission after K-Shell Excitation in HCl*, Phys. Rev. Lett. **105**, 113004 (2010).

[22] R. Bohinc, M. Žitnik, K. Bučar, M. Kavčič, L. Journel, R. Guillemin, T. Marchenko, M. Simon, and W. Cao, *Dissociation of Chloromethanes upon Resonant σ^* Excitation Studied by X-Ray Scattering*, J. Chem. Phys. **139**, 134302 (2013).

[23] R. Guillemin, S. Carniato, L. Journel, W. C. Stolte, T. Marchenko, L. El Khoury, E. Kawerk, M. N. Piancastelli, A. C. Hudson, D. W. Lindle, and M. Simon, *A Review of Molecular Effects in Gas-Phase KL X-Ray Emission*, J. Electron Spectrosc. Relat. Phenom. **188**, 53 (2013).

[24] M. N. Piancastelli, G. Goldsztejn, T. Marchenko, R. Guillemin, R. K. Kushawaha, L. Journel, S. Carniato,

J.-P. Rueff, D. Céolin, and M. Simon, *Core-Hole-Clock Spectroscopies in the Tender X-Ray Domain*, J. Phys. B **47**, 124031 (2014).

[25] U. Ankerhold, B. Esser, and F. von Busch, *Ionization and Fragmentation of OCS and CS₂ after Photoexcitation around the Sulfur 2p Edge*, Chem. Phys. **220**, 393 (1997).

[26] M. Kavčič, M. Budnar, A. Muhleisen, F. Gasser, M. Žitnik, K. Bučar, and R. Bohinc, *Design and Performance of a Versatile Curved-Crystal Spectrometer for High-Resolution Spectroscopy in the Tender X-Ray Range*, Rev. Sci. Instrum. **83**, 033113 (2012).

[27] R. C. C. Perera and R. E. LaVilla, *Molecular X-Ray Spectra: S-Kβ Emission and K Absorption Spectra of SCO and CS₂*, J. Chem. Phys. **81**, 3375 (1984).

[28] P. Glans, K. Gunnelin, P. Skytt, J.-H. Guo, N. Wassdahl, J. Nordgren, H. Ågren, F. Kh. Gel'mukhanov, T. Warwick, and E. Rotenberg, *Resonant X-Ray Emission Spectroscopy of Molecular Oxygen*, Phys. Rev. Lett. **76**, 2448 (1996).

[29] P. Glans, P. Skytt, K. Gunnelin, J.-H. Guo, and J. Nordgren, *Selectively Excited X-Ray Emission Spectra of N₂*, J. Electron Spectrosc. Relat. Phenom. **82**, 193 (1996).

[30] W. Domcke and L. S. Cederbaum, *Vibronic Coupling and Symmetry Breaking in Core Electron Ionization*, Chem. Phys. **25**, 189 (1977).

[31] A. Kivimäki, B. Kempgens, K. Maier, H. M. Köppe, M. N. Piancastelli, M. Neeb, and A. M. Bradshaw, *Vibrationally Resolved O 1s Photoelectron Spectrum of CO₂: Vibronic Coupling and Dynamic Core-Hole Localization*, Phys. Rev. Lett. **79**, 998 (1997).

[32] H. Wang, M. Bässler, I. Hjelte, F. Burmeister, and L. Karlsson, *A Vibrationally Resolved Experimental Study of the Sulfur L-Shell Photoelectron Spectrum of the CS₂ Molecule*, J. Phys. B **34**, 1745 (2001).

[33] P. Skytt, P. Glans, J.-H. Guo, K. Gunnelin, C. Såthe, J. Nordgren, F. Kh. Gel'mukhanov, A. Cesar, and H. Ågren, *Quenching of Symmetry Breaking in Resonant Inelastic X-Ray Scattering by Detuned Excitation*, Phys. Rev. Lett. **77**, 5035 (1996).

[34] A. Cesar, F. Gel'mukhanov, Y. Luo, H. Ågren, P. Skytt, P. Glans, J. Guo, K. Gunnelin, and J. Nordgren, *Resonant X-Ray Scattering beyond the Born-Oppenheimer Approximation: Symmetry Breaking in the Oxygen Resonant X-Ray Emission Spectrum of Carbon Dioxide*, J. Chem. Phys. **106**, 3439 (1997).

[35] K. Gunnelin, P. Glans, J.-E. Rubensson, C. Såthe, J. Nordgren, Y. Li, F. Gel'mukhanov, and H. Ågren, *Bond-Length-Dependent Core Hole Localization Observed in Simple Hydrocarbons*, Phys. Rev. Lett. **83**, 1315 (1999).

[36] J. D. Mills, J. A. Sheehy, T. A. Ferett, S. H. Southworth, R. Mayer, D. W. Lindle, and P. W. Langhoff, *Nondipole Resonant X-Ray Raman Spectroscopy: Polarized Inelastic Scattering at the K Edge of Cl₂*, Phys. Rev. Lett. **79**, 383 (1997).

[37] F. Gel'mukhanov and H. Ågren, *Comment on "Nondipole Resonant X-Ray Raman Spectroscopy: Polarized Inelastic Scattering at the K Edge of Cl₂"*, Phys. Rev. Lett. **82**, 666 (1999).

[38] J. D. Mills, J. A. Sheehy, T. A. Ferrett, S. H. Southworth, R. Mayer, D. W. Lindle, and P. W. Langhoff, *Mills et al. Reply*, Phys. Rev. Lett. **82**, 667 (1999).

[39] A. I. Akhiezer and V. B. Berestetski, *Quantum Electrodynamics* (Wiley-Interscience, New York, 1965).

[40] X. J. Liu, Q. Miao, F. Gel'mukhanov, M. Patanen, O. Travnikova, C. Nicolas, H. Ågren, K. Ueda, and C. Miron, *Einstein-Bohr Recoiling Double-Slit Gedanken Experiment Performed at the Molecular Level*, Nat. Photonics **9**, 120 (2015).

[41] J. L. Campbell and T. Papp, *Widths of the Atomic K-N7 Levels*, At. Data Nucl. Data Tables **77**, 1 (2001).

[42] F. Gel'mukhanov and H. Ågren, *Channel Interference in X-Ray Raman Scattering: Parity Selection Rules, Dephasing and Localization of Core Holes*, J. Electron Spectrosc. Relat. Phenom. **93**, 31 (1998).

[43] F. Gel'mukhanov, H. Ågren, and T. Privalov, Zh. Eksp. Teor. Fiz. **112**, 37 (1997) [*Restoration of Selection Rules in Nonadiabatic Resonant Inelastic X-Ray Scattering*, JETP **85**, 20 (1997)].

[44] Y. Ma, *Structure Determination Using X-Ray Fluorescence Interferometry*, Chem. Phys. Lett. **230**, 451 (1994).

[45] Y. Ma, *X-Ray Absorption, Emission, and Resonant Inelastic Scattering in Solids*, Phys. Rev. B **49**, 5799 (1994).

[46] Y. Luo, H. Ågren, F. Gel'mukhanov, J. Guo, P. Skytt, N. Wassdahl, and J. Nordgren, *Symmetry-Selective Resonant Inelastic X-Ray Scattering of C₆₀*, Phys. Rev. B **52**, 14479 (1995).

[47] M.-J. Hubin-Franskin, J. Delwiche, A. Poulin, B. Leclerc, P. Roy, and D. Roy, *Study of CS₂ in the 3-10 eV Energy Range by Electron Energy Loss Spectroscopy*, J. Chem. Phys. **78**, 1200 (1983).

[48] Ch. Jungen, D. N. Malm, and A. J. Merer, *Ultraviolet Absorption of CS₂ near the N₂ Laser Wavelengths (3371 Å)*, Chem. Phys. Lett. **16**, 302 (1972).

[49] A. Kikas, T. Käämbre, A. Saar, K. Kooser, E. Nõmmiste, I. Martinson, V. Kimberg, S. Polyutov, and F. Gel'mukhanov, *Resonant Inelastic X-Ray Scattering at the F 1s Photoabsorption Edge in LiF: Interplay of Excitonic and Conduction States, and Stokes Doubling*, Phys. Rev. B **70**, 085102 (2004).

[50] M. Kavčič, M. Žitnik, K. Bučar, A. Mihelič, B. Marolt, J. Szlachetko, P. Glatzel, and K. Kvashnina, *Hard X-Ray Absorption Spectroscopy for Pulsed Sources*, Phys. Rev. B **87**, 075106 (2013).

[51] P. S. Bagus and H. F. Schaefer, *Localized and Delocalized 1s Hole States of the O₂⁺ Molecular Ion*, J. Chem. Phys. **56**, 224 (1972).

[52] A. I. Kuleff and L. S. Cederbaum, *Ultrafast Correlation-Driven Electron Dynamics*, J. Phys. B **47**, 124002 (2014).